arXiv:1701.03288v1 [cond-mat.mes-hall] 12 Jan 2017

Coupled Yu-Shiba-Rusinov states in molecular dimers on $NbSe_2$

Shawulienu Kezilebieke,[1] Marc Dvorak,[2] Teemu Ojanen,[1,*] and Peter Liljeroth[1,†]

[1] *Department of Applied Physics, Aalto University School of Science, P.O.Box 15100, 00076 Aalto, Finland*

[2] *Centre of Excellence in Computational Nanoscience (COMP) and Department of Applied Physics, Aalto University, P.O.Box 11100, 00076 Aalto, Finland*

(Dated: January 13, 2017)

Abstract

Magnetic impurities have a dramatic effect on superconductivity by breaking the time-reversal symmetry and inducing so-called Yu-Shiba-Rusinov (YSR) low energy bound states within the superconducting gap [1–5]. These types of systems have attracted renewed interest after the recent observation of Majorana modes in a linear chain of magnetic atoms on an s-wave superconductor [6, 7]. In general, controlled coupling of YSR states should enable realizing designer quantum materials with novel topological phases [8]. The spatial extent of YSR states depends crucially on the dimensionality of the underlying superconductor and is greatly enhanced in 2D systems [9], which should facilitate the formation of coupled states. However, coupling between YSR states on 2D superconductors has not yet been demonstrated. Here, we observe YSR states on single cobalt phthalocyanine (CoPC) molecules on a 2D superconductor $NbSe_2$ and confirm their slow spatial decay using low-temperature scanning tunneling microscopy (STM) and spectroscopy (STS). We use STM lateral manipulation to create controlled CoPc dimers and demonstrate the formation of coupled YSR states. The experimental results are corroborated by theoretical analysis of the coupled states in lattice and continuum models. Our work forms an important step towards the realization of exotic topological states in designer magnetic lattices [8, 10].

A single magnetic impurity on a superconducting (SC) surface can locally modify the superconducting order parameter and induce so-called Yu-Shiba-Rusinov (YSR) states in the superconducting gap [1–4]. These states can be detected in real space by scanning tunneling microscopy (STM) and their energy spectrum has been studied in great detail by scanning tunneling spectroscopy (STS) on a variety of traditional s-wave superconductors [5, 11–15]. In addition to individual impurities, self-assembled dimers at atomic separations [11] and atomic wires of magnetic atoms have been investigated [6, 7].

Ferromagnetic coupling between the two impurities results in YSR states that hybridize and split into bonding and anti-bonding states [11, 16–18]. Atomic chains with a suitable spin-texture have been suggested to support 1D topological superconductivity [19] and Majorana modes at each end [20], which have been recently realized in iron chains on Pb(110) [6, 7]. However, the experimentally observed YSR states on s-wave superconductors (Pb and Nb) are localized within a few atomic distances from the impurity centre and their energies vary strongly depending on the adsorption site of the impurity. This greatly hampers forming assemblies of controllably coupled YSR states.

Recently, Ménard et al. demonstrated that the spatial extent of the YSR states depends on the dimensionality of the superconductor and is greatly enhanced in 2D systems, where the impurity bound state can extend over several nanometres away from the impurity [9]. This was demonstrated on iron impurities embedded into a niobium diselenide ($NbSe_2$) substrate, which is layered material with a superconducting transition at 7.2 K. Due to the weak van der Waals interaction between adjacent layers, it behaves essentially as a 2D system. In the present work, we study magnetic molecules (cobalt phthalocyanine, CoPc) on $NbSe_2$ surface and observe YSR states and with a large spatial extension. Crucially, we form controlled magnetic dimers through STM lateral manipulation and observe a hybridization of YSR states of molecules over two nanometres apart. We use continuum and lattice models for a detailed understanding of the coupling, which is a prerequisite for a realization of previously unobserved quantum states of matter such as designer topological superconductors with high Chern numbers [8].

Figure 1a shows an atomic resolution STM image of a $NbSe_2$ surface at 4.2 K. It reveals the hexagonal arrangement of the outermost Se atoms, and the well-known 3×3 charge-density wave (CDW) superstructure [9, 21]. Figure 1b displays a topographic STM image of two isolated cobalt phthalocyanine (CoPc) molecules on $NbSe_2$. We have determined

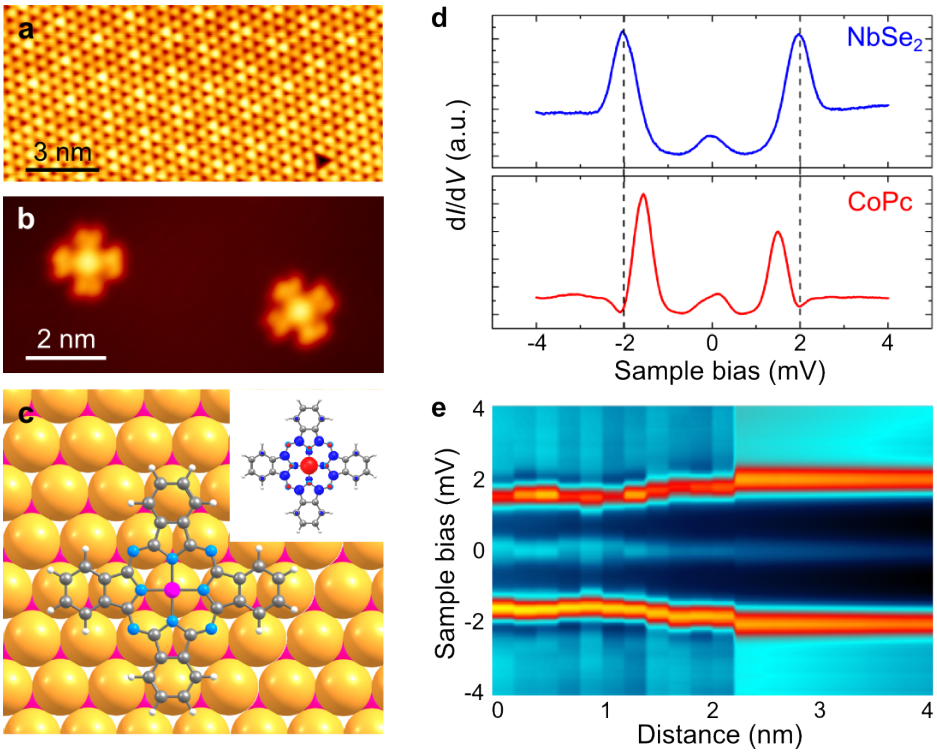

FIG. 1. **CoPc molecules deposited on $NbSe_2$ surface.** **a**, Atomically resolved STM image of the $NbSe_2$ surface. **b**, STM image of two CoPc molecules. **c**, DFT results on the CoPc adsorption on $NbSe_2$. Inset shows the calculated spin density on the CoPc molecule. **d**, Measured dI/dV spectra on the bare $NbSe_2$ substrate (top panel) and on an isolated CoPc molecule (bottom panel) with a superconducting STM tip. **e**, dI/dV spectra acquired at different distances from the centre of a CoPc molecule showing the evolution of the YSR resonances.

the adsorption site of CoPc from atomically resolved images (Supplementary Information), which is relevant as the molecular properties (e.g. spin state and more importantly, the magnetic coupling to the superconductor) might depend on this. Our STM measurements indicate that independent of the molecular orientation, the central Co atom always sits on top of an underlying Se atom. This experimentally observed adsorption configuration is confirmed by density-functional theory (DFT) calculations, with Fig. 1c showing the most stable adsorption structure.

dI/dV spectroscopy was performed with $NbSe_2$-coated SC tip to increase the energy resolution beyond the thermal limit [11, 12, 21]. Figure 1d (upper panel) shows a typical dI/dV spectrum acquired on bare $NbSe_2$ substrate. It exhibits a gap that is twice the size of the SC gap of $NbSe_2$, with sharp coherence peaks at $\pm 2\Delta \sim 2$ meV [22, 23]. The small

peak close to $V = 0$ is due to the tunneling of thermally excited quasiparticles. $\mathrm{d}I/\mathrm{d}V$ curve taken on a CoPC molecule (Fig. 1d, lower panel) shows that the coherence peaks at $\pm 2\Delta$ are replaced by pronounced peaks of asymmetric heights within the SC gap and two replicas of those peaks close to $V = 0$, similarly to an earlier report on MnPC on Pb surface [12]. These asymmetric peaks in the SC gap arise from the interaction between an isolated spin on CoPC and Cooper pairs in $NbSe_2$, i.e. the formation of YSR states. Despite CoPc adsorption being driven by the weak van der Waals forces, the magnetic coupling is still sufficiently strong to result in the formation of YSR states. DFT calculations predict that CoPC on $NbSe_2$ has the same spin as in the gas phase, $S = 1/2$. The inset of Fig. 1c shows the spin density of CoPC on $NbSe_2$ surface, which is derived from the cobalt d_{z^2} orbital, as expected.

Because of the 2D nature of $NbSe_2$, the YSR states should extend several atomic distances away from the impurity [9]. We test this behaviour by recording spectra along a line over a single CoPc as shown in Fig. 1e (zero corresponds to the centre of the molecule). Unlike magnetic impurities on 3D s-wave superconductor (Pb,Nb), where the spatial extent of YSR states is restricted to a few atomic distances, our results indicate that the YSR states extend > 2 nm away from the impurity. Therefore, these extended YSR states are ideal for the formation of coupled states.

The coupling of subgap states is illustrated in Fig. 2a, which shows schematically how two nearby YSR states hybridize and form bonding and antibonding combinations. In this case, phenomenological theory predicts a splitting that depends on the dimensionless coupling strength α (i.e the energy of an individual YSR state), the relative orientations of the two (classical) spins and the separation between the spins [4, 8, 16, 24] (Supplementary Information). α can be determined from experiments on a single impurity and we estimate a value of $\alpha \approx 0.5$. The splitting oscillates with a period determined by k_F (See Fig. 2b) and obtains its maximum value for a ferromagnetic alignment of the spins. Coupling of antiparallel spins (dotted line in Fig. 2b) does not result in energy splitting but the degenerate energy level is slightly shifted from the individual YSR energy.

Using STM lateral manipulation [25], we successfully constructed molecular dimers with different separations (see Supplementary Information for details). In all cases, we have manipulated one molecule of the dimer and have recorded the spectrum on the one which has not been moved. In this way, we have made sure that the target molecule is always

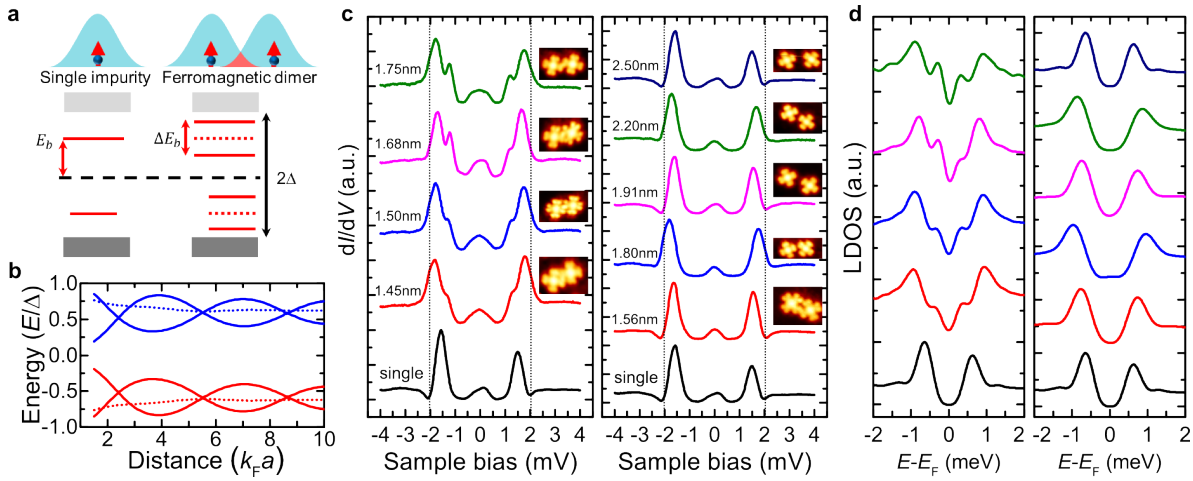

FIG. 2. **Formation of coupled YSR states on CoPc dimers.** **a**, Schematic of the formation of coupled YSR states. **b**, Calculated evolution of the YSR state energies as a function of the impurity dimer separation for a ferromagnetic (solid lines) and antiferromagnetic (dotted lines) dimer. **c**, Set of dI/dV spectra showing split (left panel) and non-split YSR states (right panel). A spectrum measured on an isolated CoPc (black line) is shown in both panels for comparison. The dotted line shows the position of the SC gap edge at $\pm 2\Delta/e$. **d**, The LDOS extracted by numerical convolution from the experimental dI/dV curves.

at the same adsorption side. Figure 2c shows point spectra on the molecular dimers with different separations (STM images of the dimers are shown in the insets). Unlike in the case of a single CoPc molecule where we observed only one pair of YSR resonances in the SC gap, now, the main YSR peaks are split to two peaks (left panel). In order to remove the influence of the superconducting density of states of the tip, numerical deconvolution was performed to directly extract the local density of states (LDOS) of the YSR states due to the CoPc molecules. Figure 2d shows the measured LDOS, where the split YRS states (left panel) can be compared to the single YSR peaks at ± 0.63 meV. It is evident that the energy positions of split peaks change depending on distance between the dimers.

We observe a maximum splitting of ~ 0.5 meV, which is very similar to the predictions from a simple continuum model for experimentally relevant distances (Fig. 2b). Magnetic coupling between the spins (through e.g. RKKY interaction) is expected to be weak compared to kT at $T = 4.2$K. Therefore the spins in a dimer are randomly oriented (thermal average). Since majority of random orientations give rise to energy splittings comparable to

the maximum splitting, we would observe experimentally essentially the same splitting as the maximum value (see Supplementary Information for details).

Other possible reasons for splitting of the YSR states include different angular momentum scattering contributions, individual d orbitals acting as separate scattering potentials or low-energy excitations due to magnetic anisotropy or vibrations [13–15, 26–29]. All of the above scenarios are predicted on a single magnetic impurity, where we always observe only a single pair of YSR states. This leaves the magnetic coupling between the impurities through the SC medium and the formation of coupled YSR states as the natural explanation of the observed spectra.

The right panel of Figure 2c shows a different set of $\mathrm{d}I/\mathrm{d}V$ spectra on the molecular dimers. While not identical, the intra-dimer distances are over a similar range as in left panel of Fig. 2c. Surprisingly, small changes in the distance result in drastic changes in the spectra and we observe alternating single and split YSR state behaviour. Once the impurity separations exceed ~ 2.5 nm, we only observe response consistent with single impurity YSR states. As indicated above, we do not expect the spins to be strictly antiparallel, and the expected distance dependence (period of k_F) is not consistent with these rapid changes between split and non-split dimer states.

In order to understand this behaviour, we have to go beyond the continuum description of the SC substrate. The Fermi surface of the $NbSe_2$ is anisotropic [30], which gives rise to star-shaped structures in the LDOS around a magnetic impurities and vortices [9]. In addition, the YSR wavefunctions have atomic scale oscillations that are potentially important for the coupling (overlap) of these states. We model these effects using a next-nearest neighbour tight-binding model [16] (see Supplementary Information for details). Calculated LDOS of a single impurity is shown in Fig. 3a. The wavefunction strongly reflects the crystal symmetry and it is easy to see that the coupling might strongly depend on the relative orientation of the dimer. We have calculated coupled dimers for different positions of the magnetic impurities and the splitting of the YSR states is shown in Fig. 3b. In addition to a very clear six-fold symmetry stemming from the crystal lattice, there are strong atomic scale variations. This is highlighted in Fig. 3c, which shows the YSR splitting as a function of the dimer separation over the experimentally relevant range. It is seen to oscillate wildly, in agreement with the experimental data (shown with solid red squares).

In Fig. 3d,e we have illustrated the bonding and antibonding wavefunctions of two

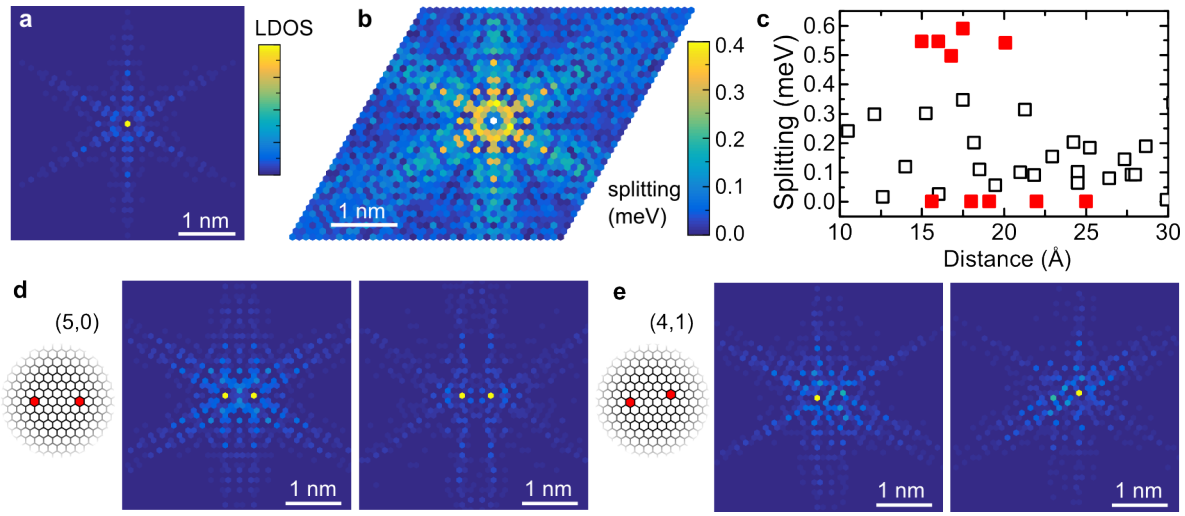

FIG. 3. **Atomic scale details of the coupling between two magnetic impurities.** **a**, Calculated LDOS of single impurity in the next-nearest neighbour tight-binding model. **b**, Calculated splitting as a function of the impurity position (the other impurity is at (0,0)). **c**, Calculated (open symbols) and measured (closed symbols) splitting of the YSR states as a function of the distance between the impurities. **d,e** Calculated bonding (left panels) and antibonding (right panels) state LDOS for a strongly coupled (5,0) (panel d) and weakly coupled (4,1) (panel e) dimer.

dimers, where one of the impurities has been moved by a single lattice site from (5,0) to (4,1) (the other impurity is at (0,0)). The calculated YSR splitting in these two dimers is 0.35 meV (5,0) and 0.02 meV (4,1). The latter is far below our experimental energy resolution and would not result in an observable splitting of the YSR resonances. The calculated wavefunctions reflect this: while they are delocalized on both impurities in the strongly coupled dimer (Fig. 3d, analogous to H_2 molecule), they are mostly localized on a single impurity in the weakly coupled dimer (Fig. 3e). This highlights that the atomic scale details are important for a detailed understanding of the coupled YSR states.

In conclusion, we have demonstrated the formation and coupling of long-range YSR states on CoPc impurities on $NbSe_2$. Using STM lateral manipulation, we have constructed well-defined CoPc dimers and observed coupled YSR states. The coupling strength depends on the dimer separation and the angle relative to the substrate lattice with strong atomic scale variations stemming from Bloch part of the wavefunctions and the resulting changes in the overlap of the two impurity states. The agreement between our observations and theoretical modelling is promising for realization of novel topological states predicted in YSR lattices.

METHODS

Sample preparation. Sample preparation and subsequent STM experiments were carried out in an ultrahigh vacuum system with a base pressure of $\sim 10^{-10}$ mbar. The $2H$–$NbSe_2$ single crystal (HQ Graphene, the Netherlands) was cleaved in situ by attaching a tape to the crystal surface and pulling the tape in vacuum in the load-lock chamber using the sample manipulator. CoPC molecules (Sigma-Aldrich) was deposited from an effusion cell held at 390°C onto a freshly cleaved $NbSe_2$ at room temperature.

STM measurements. After the CoPc deposition, the sample was inserted into the low-temperature STM (Unisoku USM-1300) and all subsequent experiments were performed at $T = 4.2$ K. STM images were taken in the constant current mode. $\mathrm{d}I/\mathrm{d}V$ spectra were recorded by standard lock-in detection while sweeping the sample bias in an open feedback loop configuration, with a peak-to-peak bias modulation of 50–100 μV at a frequency of 709 Hz.The $NbSe_2$ tip was prepared by indenting the tip into the $NbSe_2$ surface by a few nanometers while applying a voltage of 10V. Manipulation of the CoPc was carried out by placing the tip above the centre of the molecule with a bias voltage of 0.1 V and the current was increased to 1 nA with the feedback engaged. The tip was then dragged towards the desired location.

DFT calculations. Density functional theory calculations were performed with the FHI-AIMS computational package [31, 32] and the PBE generalized gradient approximation for the exchange-correlation functional [33]. We used the standard "light" numerical settings and basis sets of numeric atomic-centered orbitals tested and recommended by FHI-AIMS. Periodic $NbSe_2$ supercells were sampled with a 2×2 k-point grid centred on the Γ point. Van der Waals interactions were included by the post-SCF Tkatchenko-Scheffler correction [34]. Before computing the electronic structure, all atomic forces were relaxed to < 0.01 eV/Å.

ACKNOWLEDGEMENTS

This research made use of the Aalto Nanomicroscopy Center (Aalto NMC) facilities and was supported by the European Research Council (ERC-2011-StG No. 278698 PRECISE-NANO), the Academy of Finland through its Centres of Excellence Program (projects no.

284594 and 284621) and the Academy Research Fellow program (T.O.), and the Aalto University Centre for Quantum Engineering (Aalto CQE).

AUTHOR CONTRIBUTIONS

S.K., T.O. and P.L. conceived and planned the experiment. S.K. performed the measurements. S.K. and P.L. analysed the STM data. T.O. carried out the theoretical analysis of the system. M.D. carried out the DFT calculations. All authors jointly authored, commented, and corrected the manuscript.

* Email: teemuo@boojum.hut.fi

† Email: peter.liljeroth@aalto.fi

[1] H. Shiba, "Classical spins in superconductors," Prog. Theor. Phys. **40**, 435–451 (1968).

[2] L. Yu, "Bound state in superconductors with paramagnetic impurities," Acta Phys. Sin. **21**, 75 (1965).

[3] A. I. Rusinov, "On the theory of gapless superconductivity in alloys containing paramagnetic impurities," Sov. Phys.JETP **29**, 11016 (1969).

[4] A. V. Balatsky, I. Vekhter, and J.-X. Zhu, "Impurity-induced states in conventional and unconventional superconductors," Rev. Mod. Phys. **78**, 373–433 (2006).

[5] A. Yazdani, B. A. Jones, C. P. Lutz, M. F. Crommie, and D. M. Eigler, "Probing the local effects of magnetic impurities on superconductivity," Science **275**, 1767–1770 (1997).

[6] S. Nadj-Perge, I. K. Drozdov, J. Li, H. Chen, S. Jeon, J. Seo, A. H. MacDonald, B. A. Bernevig, and A. Yazdani, "Observation of Majorana fermions in ferromagnetic atomic chains on a superconductor," Science **346**, 602–607 (2014).

[7] M. Ruby, F. Pientka, Y. Peng, F. von Oppen, B. W. Heinrich, and K. J. Franke, "End states and subgap structure in proximity-coupled chains of magnetic adatoms," Phys. Rev. Lett. **115**, 197204 (2015).

[8] J. Röntynen and T. Ojanen, "Topological superconductivity and high Chern numbers in 2D ferromagnetic Shiba lattices," Phys. Rev. Lett. **114**, 236803 (2015).

[9] G. C. Ménard, S. Guissart, C. Brun, S. Pons, V. S. Stolyarov, F. Debontridder, M. V. Leclerc, E. Janod, L. Cario, D. Roditchev, P. Simon, and T. Cren, "Coherent long-range magnetic bound states in a superconductor," Nat. Phys. **11**, 1013–1016 (2015).

[10] G. C. Ménard, S. Guissart, C. Brun, M. Trif, F. Debontridder, R. T. Leriche, D. Demaille, D. Roditchev, P. Simon, and T. Cren, "Two-dimensional topological superconductivity in Pb/Co/Si(111)," arXiv:1607.06353 .

[11] S.-H. Ji, T. Zhang, Y.-S. Fu, X. Chen, X.-C. Ma, J. Li, W.-H. Duan, J.-F. Jia, and Q.-K. Xue, "High-resolution scanning tunneling spectroscopy of magnetic impurity induced bound states in the superconducting gap of Pb thin films," Phys. Rev. Lett. **100**, 226801 (2008).

[12] K. J. Franke, G. Schulze, and J. I. Pascual, "Competition of superconducting phenomena and Kondo screening at the nanoscale," Science **332**, 940–944 (2011).

[13] M. Ruby, F. Pientka, Y. Peng, F. von Oppen, B. W. Heinrich, and K. J. Franke, "Tunneling processes into localized subgap states in superconductors," Phys. Rev. Lett. **115**, 087001 (2015).

[14] N. Hatter, B. W. Heinrich, M. Ruby, J. I. Pascual, and K. J. Franke, "Magnetic anisotropy in Shiba bound states across a quantum phase transition," Nat. Commun. **6**, 8988 (2015).

[15] M. Ruby, Y. Peng, F. von Oppen, B. W. Heinrich, and K. J. Franke, "Orbital Picture of Yu-Shiba-Rusinov Multiplets," Phys. Rev. Lett. **117**, 186801 (2016).

[16] M. E. Flattè and D. E. Reynolds, "Local spectrum of a superconductor as a probe of interactions between magnetic impurities," Phys. Rev. B **61**, 14810–14814 (2000).

[17] D. K. Morr and J. Yoon, "Impurities, quantum interference, and quantum phase transitions in *s*-wave superconductors," Phys. Rev. B **73**, 224511 (2006).

[18] D. K. Morr and N. A. Stavropoulos, "Quantum interference between impurities: Creating novel many-body states in *s*-wave superconductors," Phys. Rev. B **67**, 020502 (2003).

[19] S. Nadj-Perge, I. K. Drozdov, B. A. Bernevig, and A. Yazdani, "Proposal for realizing Majorana fermions in chains of magnetic atoms on a superconductor," Phys. Rev. B **88**, 020407 (2013).

[20] A. Y. Kitaev, "Unpaired Majorana fermions in quantum wires," Phys.-Usp **44**, 131 (2001).

[21] S. H. Pan, E. W. Hudson, and J. C. Davis, "Vacuum tunneling of superconducting quasiparticles from atomically sharp scanning tunneling microscope tips," Appl. Phys. Lett. **73**, 2992–2994 (1998).

[22] Y. Noat, J. A. Silva-Guillén, T. Cren, V. Cherkez, C. Brun, S. Pons, F. Debontridder, D. Roditchev, W. Sacks, L. Cario, P. Ordejón, A. García, and E. Canadell, "Quasiparticle spectra of $2H$–$NbSe_2$: Two-band superconductivity and the role of tunneling selectivity," Phys. Rev. B **92**, 134510 (2015).

[23] J. G. Rodrigo and S. Vieira, "STM study of multiband superconductivity in $NbSe_2$ using a superconducting tip," Physica C **404**, 306–310 (2004).

[24] T. Meng, J. Klinovaja, S. Hoffman, P. Simon, and D. Loss, "Superconducting gap renormalization around two magnetic impurities: From Shiba to Andreev bound states," Phys. Rev. B **92**, 064503 (2015).

[25] D. M. Eigler and E. K. Schweizer, "Positioning single atoms with a scanning tunnelling microscope," Nature **344**, 524–526 (1990).

[26] A. B. Kunz and D. M. Ginsberg, "Band calculation of the effect of magnetic impurity atoms on the properties of superconductors," Phys. Rev. B **22**, 3165–3172 (1980).

[27] Michael E. Flatté and Jeff M. Byers, "Local electronic structure of a single magnetic impurity in a superconductor," Phys. Rev. Lett. **78**, 3761–3764 (1997).

[28] R. Žitko, O. Bodensiek, and T. Pruschke, "Effects of magnetic anisotropy on the subgap excitations induced by quantum impurities in a superconducting host," Phys. Rev. B **83**, 054512 (2011).

[29] D. Golež, J. Bonča, and R. Žitko, "Vibrational Andreev bound states in magnetic molecules," Phys. Rev. B **86**, 085142 (2012).

[30] K. Rossnagel, O. Seifarth, L. Kipp, M. Skibowski, D. Voß, P. Krüger, A. Mazur, and J. Pollmann, "Fermi surface of $2H$–$NbSe_2$ and its implications on the charge-density-wave mechanism," Phys. Rev. B **64**, 235119 (2001).

[31] V. Blum, R. Gehrke, F. Hanke, P. Havu, V. Havu, X. Ren, K. Reuter, and M. Scheffler, "Ab initio molecular simulations with numeric atom-centered orbitals," Comput. Phys. Commun. **180**, 2175 – 2196 (2009).

[32] V. Havu, V. Blum, P. Havu, and M. Scheffler, "Efficient integration for all-electron electronic structure calculation using numeric basis functions," J. Comput. Phys. **228**, 8367 – 8379 (2009).

[33] J. P. Perdew, K. Burke, and M. Ernzerhof, "Generalized gradient approximation made simple," Phys. Rev. Lett. **77**, 3865–3868 (1996).

[34] A. Tkatchenko and M. Scheffler, "Accurate molecular van der Waals interactions from ground-state electron density and free-atom reference data," Phys. Rev. Lett. **102**, 073005 (2009).

[35] J. Tersoff and D. R. Hamann, "Theory of the scanning tunneling microscope," Phys. Rev. B **31**, 805–813 (1985).

[36] E. W. Hudson, *Investigating high-Tc superconductivity on the atomic scale by scanning tunneling microscopy*, Ph.D. thesis, University of California at Berkeley (1999).

[37] M. Ruby, B. W. Heinrich, J. I. Pascual, and K. J. Franke, "Experimental demonstration of a two-band superconducting state for lead using scanning tunneling spectroscopy," Phys. Rev. Lett. **114**, 157001 (2015).

[38] S. Twomey, "On the numerical solution of fredholm integral equations of the first kind by the inversion of the linear system produced by quadrature," J. ACM **10**, 97–101 (1963).

[39] Y. Kim, J. Zhang, E. Rossi, and R. M. Lutchyn, "Impurity-induced bound states in superconductors with spin-orbit coupling," Phys. Rev. Lett. **114**, 236804 (2015).

SUPPLEMENTARY INFORMATION

ADSORPTION GEOMETRY OF COPC

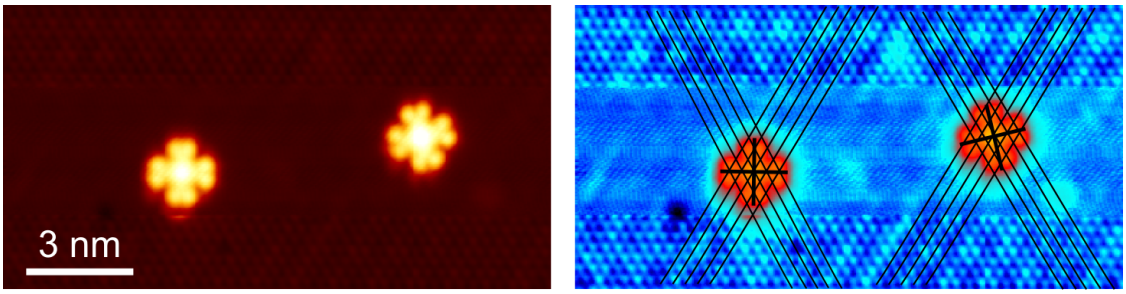

FIG. 4. **CoPc adsorption site determination.** STM image of two coPc molecules. The STM feedback current was reduced of the CoPc to avoid their accidental manipulation.

The adsorption site of CoPc can be determined from atomically resolved STM images (Fig. 4). The STM feedback current was increased at the top and bottom parts of the image to allow resolving the $NbSe_2$ lattice. While scanning over the molecules, the setpoint current was reduced in order not to accidentally manipulate the molecules. Extrapolating the atomically resolved $NbSe_2$ lattice (Se is visible) allows estimating the CoPc adsorption site. Both molecules are adsorbed with the cobalt centre directly on top of a selenium atom in agreement with the DFT calculations.

STM MANIPULATION

CoPc molecules are weakly adsorbed on the $NbSe_2$ surface, making it easy to laterally manipulate them by the STM tip (Fig. 5. We successfully constructed molecular dimers with different separations by STM manipulation. Manipulation of the CoPc was carried out by placing the tip above the centre of the molecule at 0.1 V bias voltage and increasing the current to 1 nA with the feedback engaged. The tip was then dragged towards the desired location. In order to avoid the potential variability caused by the adsorption orientation, we always manipulated one molecule of the dimer and recorded the spectrum on the one which had not been moved. In this way, we have made sure that the target molecule is always in the same adsorption configuration. Figure 5 shows a series of manipulation steps demonstrating that we only move the target molecule on the surface.

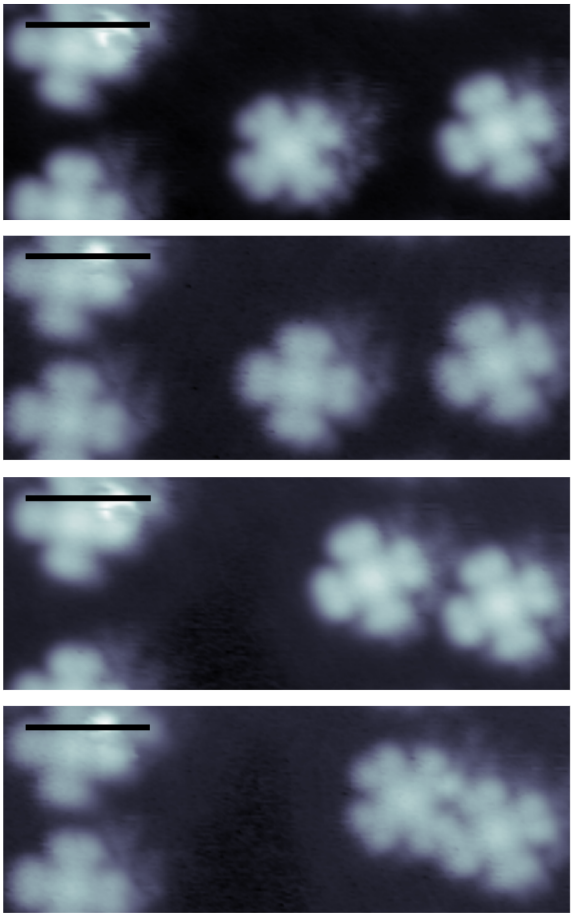

FIG. 5. **Lateral molecular manipulation of CoPc on $NbSe_2$.** Subsequent STM images of CoPc molecules after one of the molecules was laterally manipulated by the STM tip.

DECONVOLUTION OF THE DI/DV SPECTRA

The tunneling current I at bias V can be calculated from [35]

$$I(V) = \int_{-\infty}^{\infty} \rho_{\mathrm{t}}(\epsilon)\rho_{\mathrm{s}}(\epsilon + eV)\Big(f(\epsilon) - f(\epsilon + eV)\Big)d\epsilon \tag{1}$$

where ρ_{t} and ρ_{s} are the tip and substrate densities of states and f is the Fermi function. $NbSe_2$ has an anisotropic gap structure [36], which we approximated by sum of gapped DOS with some broadening and an additional gaussian component, similar to the expressions used before for modelling STM experiments with SC tips [12, 37]

$$\rho_{\mathrm{SC}}(E) = A_1 \mathrm{Re}\left(\frac{|E|}{\Big((|E| + i\gamma_1)^2 - \Delta_1^2\Big)^{1/2}}\right) + A_2 \exp(-(|E| - \Delta_2)^2/(2\gamma_2^2)) \tag{2}$$

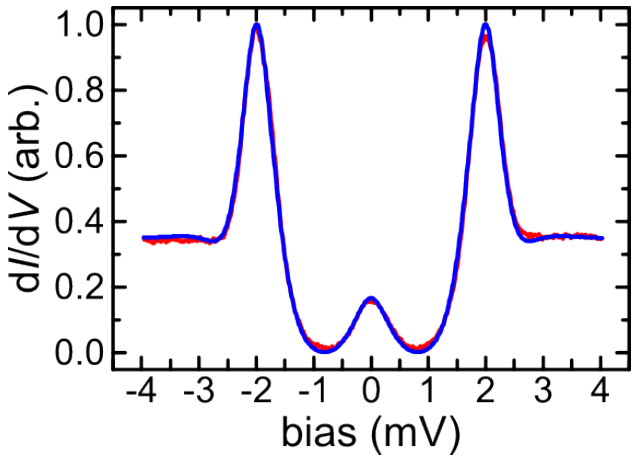

FIG. 6. **Deconvolution of the superconducting tip DOS.** Experimental $\mathrm{d}I/\mathrm{d}V$ spectrum (red line) compared with the fit to Eq. (1) (blue line) with $\Delta_1 = 0.98$ meV, $\Delta_2 = 1.01$ meV, $\gamma_1 = 0.16$ meV, $\gamma_2 = 0.27$ meV, $A_1 = 0.659$, $A_2 = 0.341$, and $T_{\mathrm{eff}} = 4.27$ K.

where $A_{1,2}$, $\Delta_{1,2}$ and $\gamma_{1,2}$ are fitted from the spectra measured on a clean $NbSe_2$ substrate with a superconducting tip. We can fit the experimental spectra extremely well as shown in Fig. 6 using the same parameters for the bulk $NbSe_2$ substrate and for the superconducting tips prepared by controlled contacts with the clean substrate. After this, using the same tip with a known ρ_{t}, we extract the substrate DOS on the CoPc molecules by a direct numerical deconvolution of Eq. (1). This is an example of a Fredholm integral equation of the first kind and can be solved numerically through a matrix equation [38].

THEORETICAL DESCRIPTION OF COUPLED MAGNETIC MOMENTS

Lattice model

In this supplement, we outline in detail the theoretical modelling of coupled Yu-Shiba-Rusinov states on the surface of $NbSe_2$. The starting point of the analysis is a lattice description of an s-wave superconductor with Hamiltonian

$$H_0 = \sum_{ij,\sigma} \frac{t_{ij}}{2}(c^\dagger_{i\sigma}c_{j\sigma} + c^\dagger_{j\sigma}c_{i\sigma}) + \sum_{i,\sigma} \Delta(c_{i\sigma}c_{i\bar{\sigma}} + c^\dagger_{i\bar{\sigma}}c^\dagger_{i\sigma}), \tag{3}$$

where t_{ii} is an on-site potential and t_{ij} $(i \neq j)$ are hopping elements between the lattice sites. The second term describes superconducting pairing of electrons with the pairing gap

Δ. The operators $c^\dagger_{i\sigma}, c_{j\sigma}$ create and destroy electrons at lattice site i with spin σ and obey the usual fermionic anticommutation relations. We assume a triangular lattice where the band structure of $NbSe_2$ can be reproduced by an appropriate choice of parameters t_{ij}. The magnetic impurities are assumed to be local and described by the Hamiltonian

$$H_{\rm imp} = -J_1 \mathbf{S}_1 \cdot C^\dagger_{n_1} \sigma C_{n_1} - J_2 \mathbf{S}_2 \cdot C^\dagger_{n_2} \sigma C_{n_2} + V_1 C^\dagger_{n_1} C_{n_1} + V_2 C^\dagger_{n_2} C_{n_2}, \tag{4}$$

where $J_i, \mathbf{S}_i$ are a magnetic coupling and a classical spin vector of an impurity at lattice position n_i. Here, we have introduced Pauli matrices $\sigma = (\sigma_x, \sigma_y, \sigma_z)$ and the second-quantized spinor operators $C_{n_i} = (c_{i\uparrow}, c_{i\downarrow})^T$. In addition to the magnetic coupling, the impurities may also perturb the superconductor with additional scalar potential parametrized by V_1 and V_2.

The standard method of solving the eigenstates of the Hamiltonian $H_0 + H_{\rm imp}$ is to generalize the problem to particle-hole space with the basis $\Psi_i = (c_{i\uparrow}, c_{i\downarrow}, c^\dagger_{i\downarrow}, -c^\dagger_{i\uparrow})^T$ and to diagonalize the Bogoliubov-de Gennes Hamiltonian

$$H_{\rm BdG} = \frac{t_{ij}}{2}\tau_z \otimes I_{2\times 2} + \Delta \delta_{ij} \tau_x \otimes I_{2\times 2} - J_1 \delta_{n_1 n_1} I_{2\times 2} \otimes \mathbf{S}_1 \cdot \sigma - J_2 \delta_{n_2 n_2} I_{2\times 2} \otimes \mathbf{S}_2 \cdot \sigma + V_1\, \delta_{n_1 n_1} \tau_z \otimes I_{2\times 2} + V_2 \delta_{n_2 n_2} \tau_z \otimes I_{2\times 2}, \tag{5}$$

which is a $4N_1 \times 4N_2$ matrix where N_1 and N_2 are the number of lattice sites in the direction of the primitive lattice vectors of a triangular lattice. We have solved the Bogoliubov-de Gennes problem $H_{\rm BdG}\Psi = E\Psi$ for a tight-binding model of $NbSe_2$ with a finite on-site, nearest-neighbour and next-nearest neighbour hoppings. The energy spectrum is symmetric with respect to zero with a gap 2Δ. Inside the gap we recover two pairs of states, corresponding to the bonding and antibonding combinations of individual YSR states. In the calculations presented in the main text, we have used values of -100 meV for the on-site and -125 meV for the nearest- and next-nearest neighbour hopping parameters [16] and $\Delta = 1$ meV, $J_1 S_1 = J_2 S_2 = 35$ meV, $V_1 = V_2 = 0$ on a lattice with $N_1 = N_2 = 400$.

Continuum model

To gain qualitative insight of the bound states of the coupled magnetic impurities we have also studied a 2D continuum model with a circular Fermi surface. In the continuum description the Bogoliubov-de Gennes Hamiltonian takes the form

$$H_{\rm BdG} = \varepsilon_k \tau_z \otimes I_{2\times 2} + \Delta \tau_x \otimes I_{2\times 2} - J\delta(\mathbf{r} - \mathbf{r}_1) I_{2\times 2} \otimes \mathbf{S}_1 \cdot \sigma - J\delta(\mathbf{r} - \mathbf{r}_2) I_{2\times 2} \otimes \mathbf{S}_2 \cdot \sigma, \tag{6}$$

where $\varepsilon_k = \frac{k^2}{2m} - \mu$ is the kinetic energy measured from the Fermi surface while the other terms are straightforward counterparts of those present in the lattice model. In the case of a single impurity, the standard calculation leads to a pair of subgap states with energies $E = \frac{1-\alpha^2}{1+\alpha^2}$, with the dimensionless coupling $\alpha = \pi\nu JS$ which contains the density of states at the Fermi level ν. Since we are not including a spin-orbit coupling, the single impurity results does not depend on the orientation of the impurity moment. While the two-spin problem does not admit a simple closed form analytical expression, the eigenstates can be solved, for example, by the methods of Ref. [39]. This leads to four subgap states $\pm E_1$ and $\pm E_2$ where the energy splitting $|E_1 - E_2|$ depends on the relative angle of the two impurity moments. The splitting is maximal for parallel moments and vanishes for antiparallel moments. As illustrated in Fig. 7, the intermediate cases interpolate between the two cases in a nonlinear manner. Thus one expects a four-peak structure even when the spins are randomly oriented. Due to the slow decay $\sim \frac{1}{\sqrt{r}}$ of 2D Shiba wavefunctions for distances smaller than the superconducting coherence length, the splitting decays slowly. Finally, as the experiments and the lattice calculations reveal, the isotropic Fermi surface cannot adequately capture coupling of two moments which varies strongly in a lattice scale.

Angular averaging of the YSR splitting

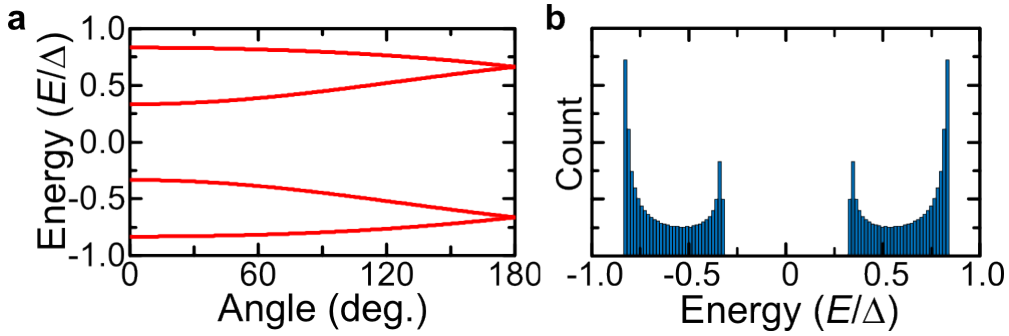

FIG. 7. **Angular averaging of the YSR splitting.** **a**, YSR state energies as a function of the angle of the magnetic moments of the two impurities according to the continuum model ($k_{\mathrm{F}}a = 3.8$, $\alpha = 0.5$). **b**, Same data presented as a histogram, which shows that majority of the angles result in a YSR splitting very close to the maximum value. This would result in clearly split resonances in the experimental spectra.